Nanoscale

PAPER

Check for updates

Cite this: *Nanoscale*, 2022, **14**, 17641

Ultra-stable blue-emitting lead-free double perovskite Cs_2SnCl_6 nanocrystals enabled by an aqueous synthesis on a microfluidic platform†

Xiaobing Tang,[a] Xiyu Wen[b] and Fuqian Yang *[a]

Received 4th October 2022,
Accepted 25th October 2022

DOI: 10.1039/d2nr05510d

rsc.li/nanoscale

Blue emitting Sn-based lead-free halide perovskite nanocrystals (NCs) are considered to be a promising material in lighting and displays. However, industrialised fabrication of blue-emitting NCs still remains a significant challenge due to the use of toxic solvents and optical instability, not mentioning in large-scale synthesis. In this work, a green-route synthesis of blue-emitting lead-free halide perovskite Cs_2SnCl_6 powders is developed, in which deionized water with a small amount of inorganic acid is used as the solvent and the synthesis of the Cs_2SnCl_6 powders is achieved on a microfluidic platform. Using the Cs_2SnCl_6 powders, we prepare Cs_2SnCl_6 NCs *via* an ultrasonication process. Changing the volume ratio of the ligands (oleic acid to oleylamine) can alter the photoluminescence (PL) characteristics of the prepared NCs, including the PL-peak wavelength, PL-peak intensity and quantum yield. The highest photoluminescence quantum yield (PLQY) of 13.4% is achieved by the Cs_2SnCl_6 NCs prepared with the volume ratio of oleic acid to oleylamine of 40 μL to 10 μL. A long-term PL stability test demonstrates that the as-synthesized Cs_2SnCl_6 NCs can retain a stable PLQY over a period of 60 days. This work opens up a new path for a large-scale green-route synthesis of blue-emitting Sn-based lead-free NCs, such as Cs_2SnX_6 (Cl, Br and I), towards their applications in optoelectronics.

1. Introduction

Blue light, as an indispensable part of full-colour displays, is of crucial importance in the areas of lighting and displays. Blue-emitting quantum dots (semiconductor nanocrystals (NCs)) have potential applications in optoelectronics, bio-imaging and so forth, because they have a wide range of merits including high brightness, a narrow full-width at half-maximum (FWHM) of photoluminescence (PL) spectrum, high colour purity, facile synthesis, *etc*. For the past few years, many efforts have been focused on the synthesis of lead halide perovskite (LHP) NCs due to their high light absorption coefficient and high defect tolerance.[1–3] However, the reported blue LHP NCs showed severe agglomeration and caused a red shift of light emission in a short time, resulting in significant optical instability. For example, Bi *et al.*[4] demonstrated that the PL-peak wavelength of blue-emitting $CsPbBr_3$ NCs changed from 470 nm to 500 nm in 12 min and the PL-peak wavelength of the modified NCs remained at 470 nm with PL stability for only 1 h. Also, the toxic lead (Pb) element in the LHP NCs causes a barrier for their large-scale applications and commercialization.

As an alternative, lead-free halide perovskite (LFHP) NCs are considered to be promising materials to replace the LHP NCs, among which, tin (Sn) (isovalent congener of lead)-based LFHP NCs have shown tremendous potential with decent optical characteristics and performance,[5,6] because compared with Pb-based perovskites, Sn-based perovskite counterparts have narrower bandgaps and higher charge mobilities.[7] However, Sn-based perovskites have poor environmental stability, resulting from the fact that partial Sn^{2+} can be easily oxidized to Sn^{4+}.[7,8] The more air-stable Sn^{4+} introduces a p-type self-doping effect and further degrades the photophysical properties of perovskites.[7–9] Recently, several antioxidants were used to improve the stability of Sn-based perovskites and the corresponding devices.[10,11] However, improving the environmental stability of Sn-based LFHP NCs still remains challenging.

Several methods have been developed to synthesize blue-emitting Sn-based LFHP NCs. Hot injection (HI) is a favorable method for the synthesis of high-quality NCs with relatively uniform sizes. This method requires the synthesis under harsh conditions, including high temperature and vacuum for the formation of NCs.[12] Also, the HI approach uses toxic and

[a]*Materials Program, Department of Chemical and Materials Engineering, University of Kentucky, Lexington, KY 40506, USA. E-mail: fuqian.yang@uky.edu*
[b]*Center for Aluminium Technology, University of Kentucky, Lexington, KY 40506, USA*

† Electronic supplementary information (ESI) available. See DOI: https://doi.org/10.1039/d2nr05510d

volatile solvents, such as 1-octadecene (ODE), which impedes the industrialization of blue-emitting Sn-based LFHP NCs from a sustainable view. To address this issue, an aqueous-solution-based green synthesis route without the use of toxic solvents is a preferable choice. Tan *et al.*[13] reported a solvothermal method for the synthesis of Bi-doped Cs_2SnCl_6 NCs with light emission at 455 nm. This method avoids the use of toxic solvents, while it requires the synthesis to be performed at a high temperature of about 200 °C. It is also challenging to control the morphology and size of the prepared NCs due to that the formation of NCs was realized by a "random" cooling process from a high temperature.[13] It should be noted that all the methods mentioned above are suitable for a small-scale synthesis of blue-emitting LFHP NCs and may not be suitable for large-scale production to achieve the industrialization and commercialization of blue-emitting Sn-based LFHP NCs.

Microfluidics has been demonstrated to be a reliable and powerful technique for large-scale manufacturing of nanoparticles and nanocrystals.[14–16] Compared with the small-scale synthesis of materials for fundamental research, microfluidics can provide continuous fabrication of materials and eliminate the samples' irreproducibility originating from batch-to-batch fabrication.[17–19] Currently, microfluidics is used to synthesize Pb-based NCs.[20,21] For example, Lignos *et al.*[20] produced all-inorganic perovskite $CsPbX_3$ (X = Cl, Br, I) NCs with the PL-peak wavelength ranging from 470 to 690 nm *via* microfluidics. Bao *et al.*[21] combined microfluidics with an inkjet printing technique to synthesize $CsPbBr_3$/Cs_4PbBr_6 nanocrystals for mini-LEDs. Recently, Xu *et al.* achieved a large-scale synthesis of cesium lead halide perovskite NCs.[22,23] However, it still remains challenging to synthesize Sn-based LFHP NCs with an aqueous solution *via* a microfluidic platform.

Realizing the challenges faced in the synthesis of blue-emitting Sn-based LFHP NCs and the practical applications of blue-emitting Sn-based LFHP NCs in optoelectronics, we developed a green approach to produce blue-emitting Sn-based LFHP (Cs_2SnCl_6) NCs using a microfluidic platform and ultrasonication consecutively. The blue-emitting Cs_2SnCl_6 NCs exhibited a PL-peak centred at 435 nm with the highest PLQY of 13.4% and good long-term optical stability over a period of 60 days.

2. Experimental section

2.1 Materials

The chemicals used in this work were CsCl (99.9%, Alfa Aesar), $SnCl_2$ (Sigma Aldrich), oleylamine (OAm) (>50%, TCI America), oleic acid (OA) (Ward's Science), a silicone elastomer base/curing agent, (Sylgard™ 184, Electron Microscopy Sciences), hexane (Sigma Aldrich), HCl acid (37%), toluene (VWR International LLC, 99.5%), isopropanol (IPA) (VWR International LLC, 99%), dichloromethane (BeanTown Chemical, 99.5%) and deionized (DI) water. No further purification was performed for all the received chemicals. HCl acid was diluted to 18.5% prior to use.

Cs_2SnCl_6 powders were first prepared. Specifically, 5 mmol CsCl powder and 5 mmol $SnCl_2$ powder were dissolved in 5 ml of water and 5 ml of HCl acid (18.5%), respectively, to produce a CsCl solution and a $SnCl_2$ solution. A microfluidic platform was assembled for the synthesis of Cs_2SnCl_6 powder at room temperature (Fig. 1). The CsCl solution and $SnCl_2$ solution were loaded in two syringes, respectively, which were placed on a syringe pump system (Harvard Apparatus). Both the CsCl solution (flow rate, 0.4 ml min^{-1}) and $SnCl_2$ solution (flow rate, 0.4 ml min^{-1}) were pumped into a microreactor through two capillaries (1.0 mm in inner diameter and 80 cm in length). These two solutions were mixed and reacted in the microreactor to immediately form white products (precipitates). Note that all the procedures were carried out under ambient conditions, in which Sn^{2+} was prone to be oxidized into Sn^{4+}. Eqn (1) shows the chemical reaction taking place in the microreactor

$$2Cs^+_{(aq)} + Sn^{2+}_{(aq)} + 4H^+_{(aq)} + 6Cl^-_{(aq)} + O_{2(g)} \rightarrow Cs_2SnCl_{6(s)} + 2H_2O_{(aq)}. \quad (1)$$

The suspension with as-formed white precipitates flowed into another capillary tube (1.6 mm in inner diameter and 20 cm in length), which connected the microreactor to a container, for the collection of the white precipitates at a total flow rate of 0.8 ml min^{-1}. The collection of white precipitates by using the microfluidic system is presented in Movie S1 in the ESI,† which shows that a white Cs_2SnCl_6 precipitate suspension continuously flows through the capillary tube to a small vial for the collection of the white Cs_2SnCl_6 precipitates, and demonstrates the feasibility of the large-scale synthesis of the Cs_2SnCl_6 precipitates (powders). Moderate amounts of the white precipitates were put onto a glass plate at 30 °C for 1 h to obtain dry white powders. Using the microfluidic system, we were able to produce 0.06 g of dry Cs_2SnCl_6 powders within 8 min (Fig. S1, ESI†) with a production rate of 0.45 g h^{-1}. Note that this result reveals that the large-scale synthesis of Cs_2SnCl_6 perovskites by microfluidics is feasible and the production rate of 0.45 g h^{-1} is only for the microfluidic system used in this work.

A mixture of 5 mg of the white powders, 5 ml of hexane and 50 μL ligands (mixture of OA and OAm) was placed in a 20 ml vial in a water bath, and was sonicated for 400 min at room

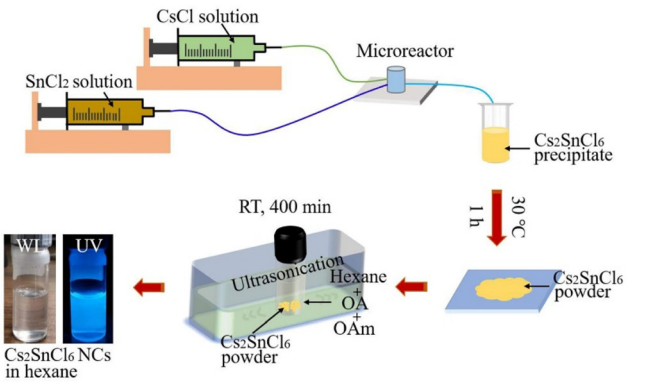

Fig. 1 Schematic of the synthesis route of Cs_2SnCl_6 NCs.

This journal is © The Royal Society of Chemistry 2022

temperature (RT). The solution with Cs_2SnCl_6 NCs was obtained by collecting the supernatant of the solution after ultrasonication. It should be pointed out that no calculation of the production rate of the Cs_2SnCl_6 NCs derived from the Cs_2SnCl_6 powders was performed, since it was very difficult, if not impossible, to dry the oily ligands on the NCs and to determine the production rate of the Cs_2SnCl_6 NCs. Different volume ratios (VRs) of OA to OAm (40 μL to 10 μL, 30 μL to 20 μL, 25 μL to 25 μL, 20 μL to 30 μL, and 10 μL to 40 μL) were used in the preparation of the mixtures. All the preparation and synthesis processes were performed under ambient conditions. The as-obtained Cs_2SnCl_6 NCs in the solution emit blue light under ultraviolet (UV) light (365 nm) and do not emit light under white light (WL) (Fig. 1).

2.2 Characterization

XRD (X-ray diffraction) measurements were carried out on an X-ray diffractometer (Bruker-AXS D8 Discover) with CuKα radiation at 1.54060 Å in wavelength. PL measurements were performed under UV light at a wavelength of 365 nm on a Horiba Scientific Fluoromax Plus-C fluorometer, and PLQY tests were performed on a Horiba Scientific Fluoromax Plus-C fluorometer equipped with an integrated sphere. The Horiba Scientific FluorEssence™ software was used in the PLQY calculation. UV stability tests were performed on a UV Stratalinker (model 1800) with 254 nm UV light bulbs.

PL lifetime decay measurements were performed using a DeltaHub™ high throughput time correlated single photon counting (TCSPC) controller and a NanoLED-350 pulsed excitation source (excitation wavelength 350 ± 10 nm). The decay curves were analysed using the Horiba Scientific decay analysis software DAS6. High-angle annular dark-field scanning transmission electron microscopy (HAADF-STEM) and high-resolution transmission electron microscopy (HRTEM) (Thermo-scientific Talos F200X operated at an accelerating voltage of 200 kV) were used to analyze the morphologies and structures of the Cs_2SnCl_6 NCs. The compositional analysis of the Cs_2SnCl_6 NCs was conducted on an energy dispersive X-ray (EDX) spectroscope (a Thermo-scientific Super-X System with four windowless silicon-drift-detectors installed on a Talos F200X TEM).

3. Results and discussion

The composition and structure of the as-prepared Cs_2SnCl_6 powders were analysed by XRD. Fig. 2a shows the XRD pattern (bottom) of the freshly prepared Cs_2SnCl_6 powder. It is evident that the XRD pattern matches well with the standard JCPDS card (PDF#00-007-0197), which indicates that the Cs_2SnCl_6 powders have a cubic structure with a point group of $Fm\bar{3}m$. This result is in good agreement with the report given by Zhang *et al.*[24] The characteristic peaks centred at 24.2°, 29.8°, 34.5° and 42.6° correspond to the (220), (222), (440) and (422) crystal planes of cubic Cs_2SnCl_6, respectively. There is a small diffractive peak centred at 32.8°, which matches with the standard JCPDS card (PDF# 00-030-0370), revealing the presence of a small amount of $CsSn_2Cl_5$ in the Cs_2SnCl_6 powders. $CsSn_2Cl_5$ was formed through the chemical reaction of Sn^{2+} with Cs^+ and Cl^- in aqueous solution. Compared with the XRD pattern of the freshly prepared Cs_2SnCl_6 powders, the XRD pattern of the Cs_2SnCl_6 powder exposed to air under ambient conditions for 50 days does not show any shifts of the peaks and any new peaks. The peak intensities for both the fresh powders and the powders exposed to air for 50 days remain almost the same. Note that there exists peak splitting of the XRD patterns in both the fresh and 50-day specimens. The peak splitting may be due to the lattice interpenetration,

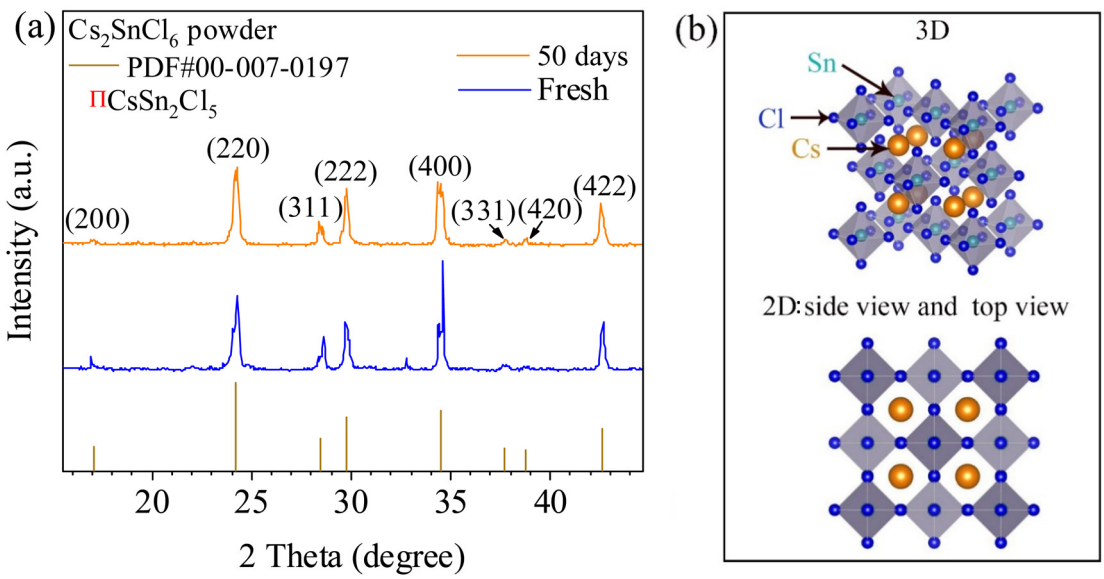

Fig. 2 (a) XRD patterns of the Cs_2SnCl_6 powder, and (b) crystal structure of the cubic Cs_2SnCl_6 perovskite in 3D and 2D views.

which may lead to the changes in the symmetry of the cubic phase.[25] These results suggest the good structural stability of the Cs_2SnCl_6 powder. It is worth noting that the impurity ($CsSn_2Cl_5$) disappears after 50 days, which suggests the inferior structural stability of $CsSn_2Cl_5$ compared with that of Cs_2SnCl_6.

The SEM image in Fig. S2 (ESI)† shows the morphology of the as-synthesized Cs_2SnCl_6 powders, which are octahedral, in agreement with the report by Zhang *et al.*[26] The EDS results (Fig. S3 and Table S1 in the ESI†) reveal that the atomic ratio of Cs : Sn : Cl is 19.79 : 11.30 : 68.92, which is close to the stoichiometric ratio of 2 : 1 : 6. This result further confirms that the as-prepared powders are Cs_2SnCl_6.

The crystal structure of a cubic Cs_2SnCl_6 perovskite is shown in Fig. 2b, in which the top and bottom layers are illustrated in 3D and 2D views, respectively. In the 3D view, the Cs_2SnCl_6 crystal contains $[SnCl_6]^{2-}$ octahedra coordinating with an alkali metal cation (Cs^+). In octahedral $[SnCl_6]^{2-}$, Sn^{4+} is shared with six Cl^- atoms. The crystal structure of Cs_2SnCl_6 can be considered in a way that a B-site cation in a double perovskite ($A_2B'B''X_6$) is replaced with a vacancy. Therefore, Cs_2SnCl_6 can be represented as $A_2B\square X_6$ and called vacancy-ordered double perovskites.[27] It looks like that every other $[BX_6]^{2-}$ octahedron is removed in a ABX_3 cubic perovskite.

The image in the bottom of Fig. 2b presents a 2D side (top) view of the crystal structure of the cubic Cs_2SnCl_6 perovskite. For a cubic structure, the top- and side-views of the crystal structure are the same. The dark and light grey squares represent the $[SnCl_6]^{2-}$ octahedra, which are not in the same plane.

The Cs_2SnCl_6 NCs were fabricated by a subsequent ultrasonication of the Cs_2SnCl_6 powders in a hexane solution consisting of OA and OAm. Fig. 3a schematically illustrates the process, in which the Cs_2SnCl_6 powders of large sizes (micro-

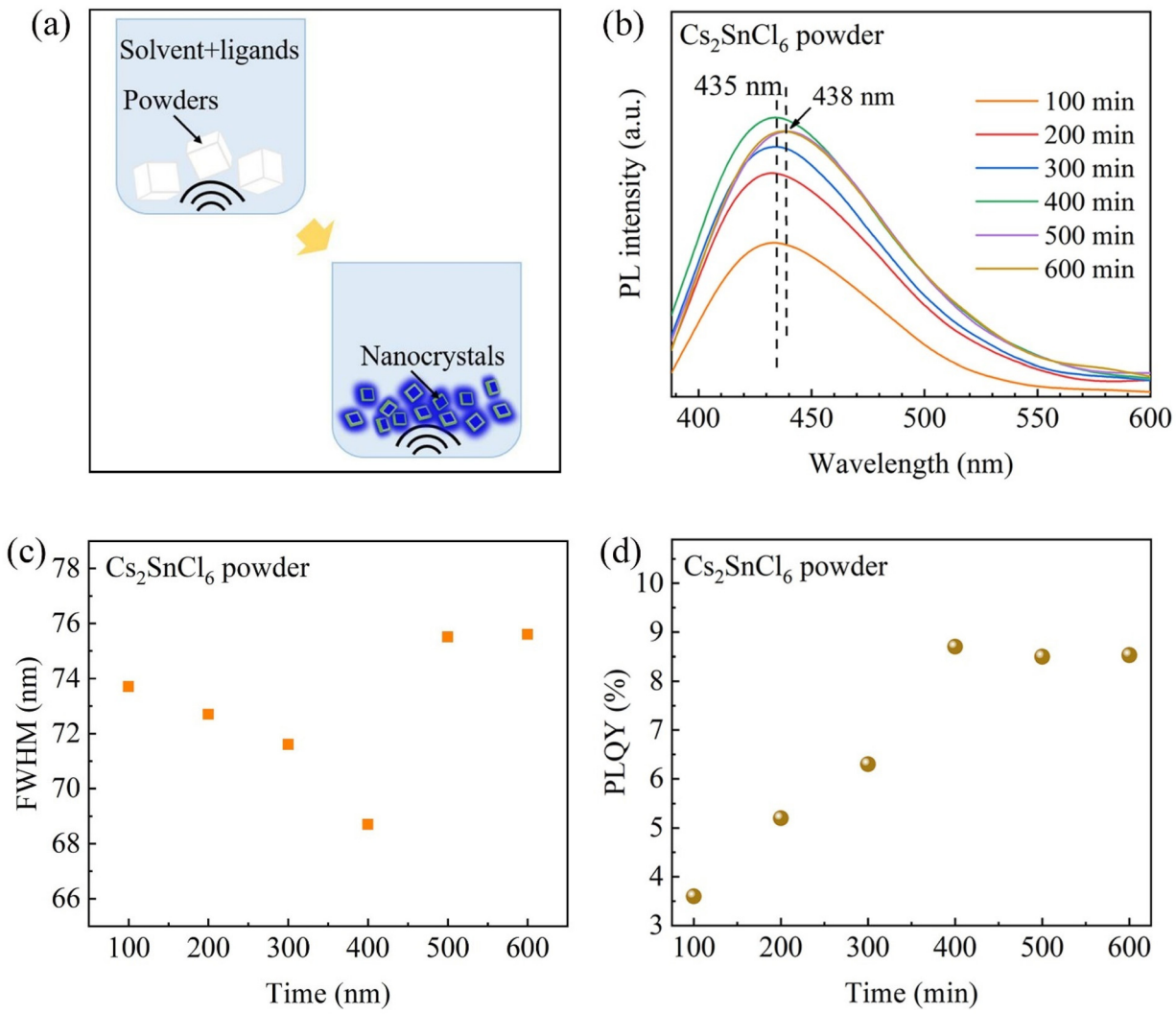

Fig. 3 (a) Schematic of ultrasonication for the preparation of Cs_2SnCl_6 NCs; (b) PL spectra and (d) PLQY of the Cs_2SnCl_6 NC solution derived from the Cs_2SnCl_6 powders in hexane solution consisting of OA and OAm (VR is 40 : 10) under ultrasonication for 100–600 min, and (c) FWHM of the spectra in (b).

This journal is © The Royal Society of Chemistry 2022

crystals) are fragmented into NCs under ultrasonication. During ultrasonication, the Cs_2SnCl_6 powders of large sizes experience dynamic deformation and absorb acoustic energy. Increasing the absorbed energy causes the cracking of the powders and the crack grows through the powders, eventually leading to the cracking of the powders.[28] Such processes occur over and over again; consequently, small NCs are formed. Note that the ultrasonic wave-derived force on a particle is proportional to the volume of the particle.[29]

Ligands (mixture of OA and OAm) play an inevitable role in the formation of NCs. The ligands wrap the formed NCs during ultrasonication to produce more and more NCs in the solution and limit the agglomeration of the NCs. OA as a capping agent on the surfaces of NCs helps to stabilize the morphology (or shape) of NCs,[30] and OAm is beneficial for the formation of smaller crystals.[31] It was reported that bulk crystals were usually formed without the use of amines when synthesizing perovskite NCs.[32] Note that OAm can increase the binding between OA and the NCs, which contributes to the PLQY increase of the NCs, as reported by De Roo *et al.*[33] These results suggest a synergistic effect between OA and OAm, which not only helps the formation of NCs but also enhances the optoelectronic characteristics of the NCs.

Fig. 3b shows the PL spectra (at an excitation wavelength of 365 nm (Fig. S4, ESI†)) of the Cs_2SnCl_6 NC solutions derived from the Cs_2SnCl_6 powders with a VR of 40 : 10 for different ultrasonication times of 100, 200, 300, 400, 500 and 600 min, respectively. It is evident that the PL intensity of the peak centred at 435 nm increases with increasing ultrasonication time. The FWHMs of the PL spectra in Fig. 3b are shown in Fig. 3c. For the ultrasonication time in a range of 100–600 min, the FWHMs of the PL spectra of the Cs_2SnCl_6 NC solutions decrease from ~73.7 to ~68.7 nm with increasing ultrasonication time from 100 to 400 min and then increase to ~75.5 and ~75.6 nm for the ultrasonication times of 500 and 600 min, respectively. The PL results are qualitatively in good accord with the PLQY trend shown in Fig. 3d. The PLQYs of the Cs_2SnCl_6 NC solutions are 3.6, 5.2, 6.3, and 8.7% after the solutions with Cs_2SnCl_6 powders were ultrasonicated for 100, 200, 300, and 400 min, respectively. It should be noted that no blue shift or red shift was observed for the Cs_2SnCl_6 NCs in the solution after a series of ultrasonication procedures in a period of 100–400 min, indicating the comparable sizes of the NCs in the solution. The increases of the PL-peak intensity and PLQY can be attributed to the increase of the concentration of the Cs_2SnCl_6 NCs in the solution. If strong photon scattering due to a high concentration of NCs is negligible, more photons are emitted from the same excitation volume in the solution, leading to the increase of the PL-peak intensity. The PLQY, η, can be calculated as[13]

$$\eta = \frac{\int I_{\text{sample}} - \int I_{\text{black}}}{N_{\text{ex}}} \quad \text{with} \quad N_{\text{ex}} = \int I_{\text{ex,black}} - \int I_{\text{ex,sample}} \quad (1)$$

where N_{ex} is the number of photons emitted from the excitation light source, I_{sample} and I_{black} are the emission (PL) intensity of the specimen and black sample, respectively, and $I_{\text{ex,black}}$ and $I_{\text{ex,sample}}$ are the emission intensity of the excitation light from the specimen and black sample, respectively. For a measurement system, I_{black} and N_{ex} are constants. Eqn (1) indicates the increase of the PLQY (η) with the increase of the PL intensity of the specimen (I_{sample}). Therefore, a higher concentration of the NCs leads to a higher PLQY.

On comparing the PL spectra of the NC solution ultrasonicated for 500 and 600 min with the PL spectrum of the same NC solution ultrasonicated for 400 min, we note slight decreases in the PL intensity and a small red shift of 3 nm of the PL peak. Correspondingly, the PLQY of the NC solution decreases to 8.5% (500 min) and 8.53% (600 min). Such results suggest that the photon scattering in the NC solution ultrasonicated for 500 and 600 min is likely not negligible. The red shift might be caused by the size effect (size increase) of the NCs due to agglomeration.

The absorbance spectra of the Cs_2SnCl_6 NC solutions prepared from the Cs_2SnCl_6 powders (the VR is 40 : 10) under ultrasonication for 100–400 min are presented in Fig. S5 (ESI†). Consistent with the PL intensity shown in Fig. 3b, the absorbance of the NC solutions increases with the increase of the ultrasonication time to 400 min, indicating the increase in the concentration of the Cs_2SnCl_6 NCs in the solution. Note that the increase of the PLQY can also be attributed to the quantum size effect when the average NC size becomes smaller.[34]

To examine if there exists the quantum size effect, we performed HAADF-STEM imaging of the sizes of the Cs_2SnCl_6 NCs. Fig. 4a shows a HAADF-STEM image of the 400 min-ultrasonicated Cs_2SnCl_6 NCs, as represented by the white spots. Fig. 4b shows the size distribution of the Cs_2SnCl_6 NCs with an average size of ~2.49 nm, which is comparable to an average size of ~2.52 nm for the 100 min-ultrasonicated NCs (Fig. S6a and b, ESI†). This result suggests that there is no significant size effect on the PLQY enhancement which supports the result that no shift of the PL peak is observed in Fig. 3b for the ultrasonication time up to 400 min. This also indicates that the passivation of the ligands (OA and OAm) has an insignificant effect on the PLQY enhancement of the NCs because the concentration of surface defects of a NC is mainly dependent on the NC size.

The lattice fringe determined from a typical HRTEM image (inset, upper corner in Fig. 4a) is 3.71 Å in size, which corresponds to the (220) crystal plane and is in accord with the corresponding SAED (selected area electron diffraction) pattern of cubic Cs_2SnCl_6 (inset, the lower corner in Fig. 4a. For an enlarged view, see Fig. S6c in the ESI†). These results are consistent with the standard JCPDS card (PDF#00-007-0197). The EDX mappings in Fig. 4c–e reveal uniform distributions of the elements for the Cs_2SnCl_6 NCs shown in Fig. 4a. Note that only a few coloured spots representing the elements are present on the mappings because a short duration time was used in the EDX mappings. The NCs are so sensitive to the electron beam that a long-time exposure to the electron beam causes the decomposition of the NCs.

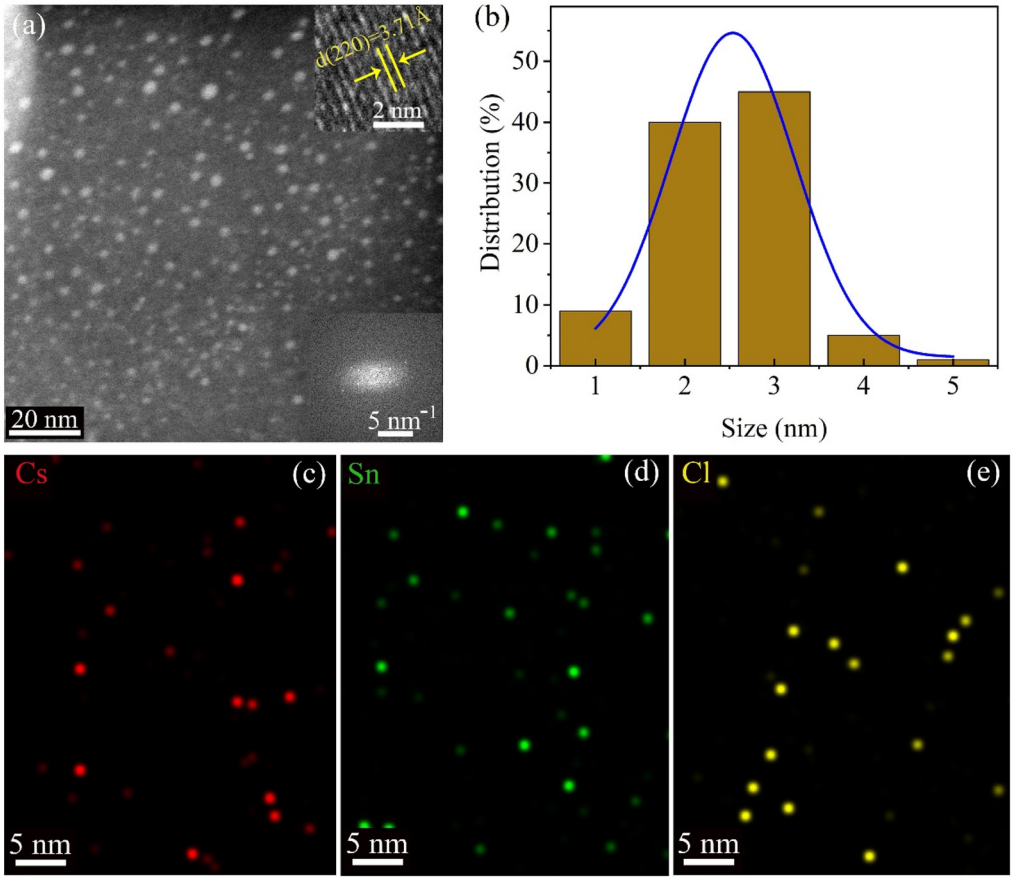

Fig. 4 (a) A HAADF-STEM image of Cs_2SnCl_6 NCs prepared with 40 : 10 of the volume ratio of OA to OAm after an ultrasonication for 400 min. Inset: a HRTEM image (upper right) and a SAED pattern (lower right), (b) size distribution of the Cs_2SnCl_6 NCs in (a), and (c–e) elemental mapping of the Cs_2SnCl_6 NCs in (a).

We used different volume ratios of OA to OAm in the synthesis of the Cs_2SnCl_6 NCs in order to examine the synergistic effect of OA and OAm on the optical characteristics of the Cs_2SnCl_6 NCs. Fig. 5a depicts the PL spectra of the Cs_2SnCl_6 NC solutions with five different volume ratios. The Cs_2SnCl_6 NC solution with a VR of 40 μL : 10 μL shows the highest PL-peak intensity with a peak wavelength of 435 nm. Decreasing the volume ratio of OA to OAm from 40 μL : 10 μL to 10 μL : 40 μL causes the decrease of the PL-peak intensity; the PL peak exhibits a slight red shift to 436 nm for the VR of 30 μL : 20 μL and then a blue shift to 429 nm for the VR of 10 μL : 40 μL. The variations of the PL-peak intensity and wavelength with the volume ratio of OA to OAm demonstrate the synergistic effect of OA and OAm on the PL characteristics of the prepared Cs_2SnCl_6 NCs. Note that the solutions prepared with only OA or OAm in hexane did not emit any light under UV light (365 nm).

The absorbance spectra of the prepared Cs_2SnCl_6 NC solutions with different volume ratios (Fig. S7, ESI†) also exhibit similar characteristics to the PL spectra. Fig. 5b shows the corresponding FWHMs of the PL spectra in Fig. 5a. The FWHM increases from ~90.0 to ~100.0 nm with the decrease of the VR of OA to OAm from 40 : 10 to 10 : 40.

Fig. 5c shows the decrease of the PLQY of the prepared Cs_2SnCl_6 NC solutions upon decreasing the volume ratio of OA to OAm, which is consistent with the decreasing trend of the PL-peak intensity with the decrease of the volume ratio of OA to OAm. Decreasing the volume ratio of OA to OAm from 40 μL : 10 μL to 10 μL : 40 μL causes the decrease of the PLQY of the Cs_2SnCl_6 NC solutions from 7.8% to 1.3%. The carrier lifetime of the Cs_2SnCl_6 NC solution also exhibits a declining trend, as revealed by the carrier lifetime decay curves in Fig. 5d.

We calculated the carrier lifetimes of the Cs_2SnCl_6 NCs by fitting the decay curves with a double exponential function as[35]

$$I_{pl} = A_1 \exp(-t/\tau_1) + A_2 \exp(-t/\tau_2) \text{ with } A_1 + A_2 = 1 \quad (2)$$

where I_{pl}, τ_1 and τ_2 are the PL-peak intensity and the carrier lifetimes of the short-lived interactive state (nonradiative recombination at the surface) and long-lived non-interactive state (radiative recombination at the core) of the Cs_2SnCl_6 NCs, respectively. A_1 and A_2 are the fractional contributions of the short-lived interactive state and long-lived non-interactive state, respectively.[35–41] Table 1 summarizes the numerical

 This journal is © The Royal Society of Chemistry 2022

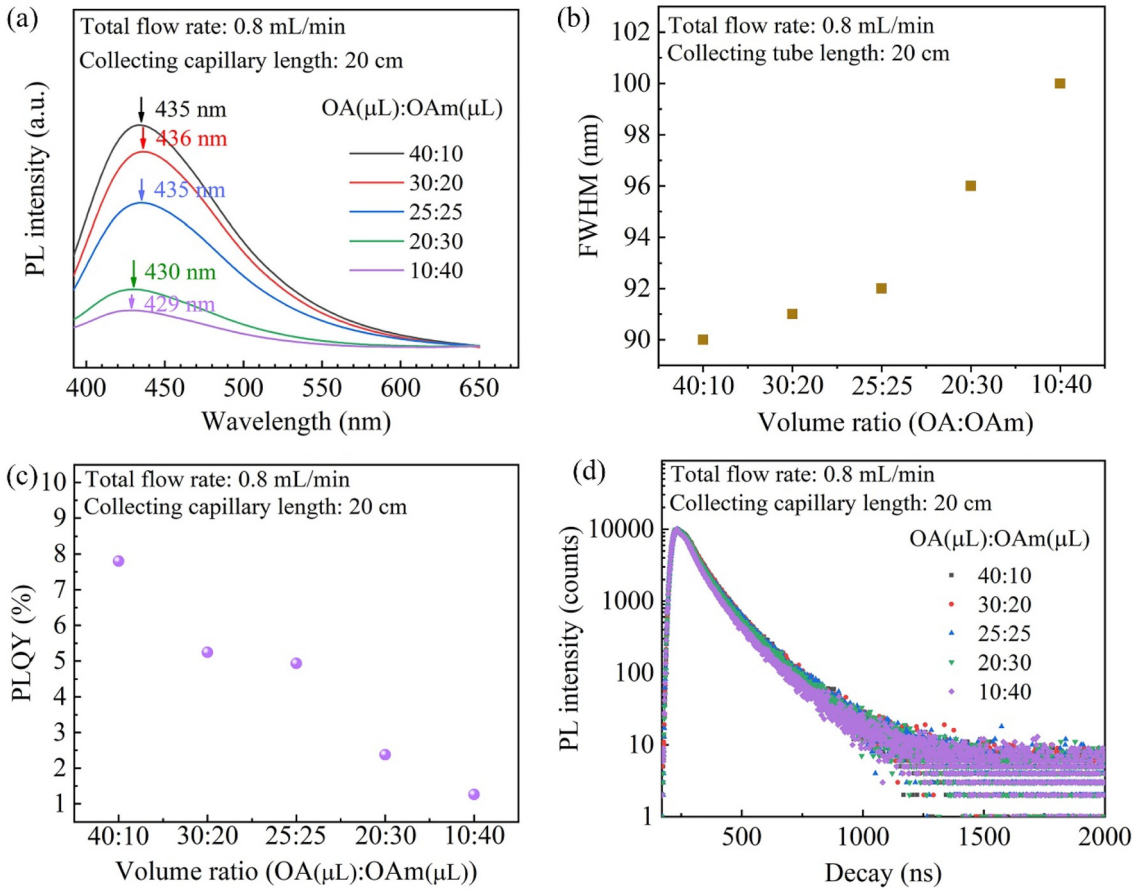

Fig. 5 (a) PL spectra, (c) PLQY, and (d) lifetime of the Cs_2SnCl_6 NC solutions prepared with different volume ratios of OA to OAm; (b) FWHM of the spectra in (a).

Table 1 Lifetimes of the Cs_2SnCl_6 NCs prepared with different volume ratios of OA to OAm in hexane

	Volume ratio				
	40 μL : 10 μL	30 μL : 20 μL	25 μL : 25 μL	20 μL : 30 μL	10 μL : 40 μL
τ_1 (ns)	3.52	3.51	3.40	3.13	2.93
τ_2 (ns)	8.18	8.16	8.08	7.77	7.49

results of τ_1 and τ_2. Both the τ_1 and τ_2 values decrease with the decrease of the volume ratio of OA to OAm. This can be attributed to the loss of the passivation of OA on the surfaces of the NCs, which leads to an increase of the surface trap density.

The wavelength effects of the excitation light on the PL characteristics of the Cs_2SnCl_6 NCs were investigated using light at excitation wavelengths of 290, 315, 340, and 365 nm. The study was focused on the Cs_2SnCl_6 NC solution with the 40 : 10 volume ratio of OA to OAm, since this Cs_2SnCl_6 NC solution exhibited the best PL performance. Fig. S8 (ESI)† depicts the PL spectra of the Cs_2SnCl_6 NC solution with and without the excitation light at excitation wavelengths of 290, 315, 340, and 365 nm. Note that the intensities of the excitation lights are so strong that the intensities of the emitting lights are not clearly observable, as shown in Fig. S8a† with both the excitation and emitting light. Fig. S8b† shows the PL spectra of the Cs_2SnCl_6 NC solution without the excitation light. It is evident that there are four emitting lights at 581, 631, 423 and 435 nm excited by the lights at 290, 315, 340, and 365 nm, respectively. The mechanism for such behavior is unclear. The presence of the emitting lights at different emission wavelengths (423 and 435 nm) might be due to the bandgap change of the Cs_2SnCl_6 NCs associated with the difference in the electron concentrations[42] at various excitation wavelengths. It is interesting to note that there are two strong emissions centred at 581 and 631 nm with narrow FWHMs at the excitation light wavelengths of 315 and 290 nm, respectively, which can be likely attributed to an artifact of the measurements.

The PL characteristics of the Cs_2SnCl_6 NCs from the Cs_2SnCl_6 powders prepared with different total flow rates and

the lengths of the capillary tube were also examined to illustrate the possible effects of the total flow rate and the length of the capillary tube. Fig. S9a and b (ESI)† show the PL spectra of the Cs_2SnCl_6 NC solutions from the Cs_2SnCl_6 powders prepared with different VRs and two different capillary lengths of 20 cm and 60 cm at a total flow rate of 0.4 mL min^{-1}. Similar to the PL characteristics of the Cs_2SnCl_6 NC solution from the Cs_2SnCl_6 powders prepared with a total flow rate of 0.8 mL min^{-1} and a capillary length of 20 cm, the PL peaks of the NC solutions prepared with a total flow rate of 0.4 mL min^{-1} and a capillary length of 20 cm exhibit a slight red shift of 2 nm first and a subsequent blue shift to 429 nm when the volume ratio of OA to OAm is decreased from 40 : 10 to 10 : 40; the PL peaks of the NC solutions prepared with a total flow rate of 0.4 mL min^{-1} and a capillary length of 60 cm exhibit a red shift first from 435 nm to 439 nm and then a blue shift from 439 nm to 429 nm when the volume ratio of OA to OAm is decreased from 40 : 10 to 10 : 40. These results are in good agreement with the corresponding PLQY results. As shown in Fig. S10a and b (ESI),† decreasing the volume ratio of OA to OAM from 40 : 10 to 10 : 40 causes the decreases of the PLQYs from 6.17% to 0.6% for the Cs_2SnCl_6 NC solutions from the Cs_2SnCl_6 powders prepared with the total flow rate of 0.4 mL min^{-1} and the capillary length of 20 cm and 6.15% to 0.83% for the Cs_2SnCl_6 NC solutions from the Cs_2SnCl_6 powders prepared with the total flow rate of 0.4 mL min^{-1} and the capillary length of 60 cm. Fig. S11a and b (ESI)† show the lifetime decay curves of the Cs_2SnCl_6 NC solutions with different volume ratios of OA to OAm, which were prepared from the Cs_2SnCl_6 powders synthesized with a total flow rate of 0.4 mL min^{-1} and two capillary lengths of 20 cm and 60 cm, respectively. The carrier lifetimes of the Cs_2SnCl_6 NCs are summarized in Tables S2 and3 (ESI).† According to the results, we can conclude that changing the total flow rate and the capillary length has insignificant effects on the PL, PLQY and carrier lifetimes of the prepared Cs_2SnCl_6 NCs.

Moreover, $(\lambda, \tilde{\tau}_1, \tilde{\tau}_2) = [(\eta,\tau_1,\tau_2)|_{VR\,=\,40:10} - (\eta,\tau_1,\tau_2)|_{VR\,=\,10:40})]/(\eta,\tau_1,\tau_2)|_{VR\,=\,10:40}$, in which the subscript represents the volume ratio of OA to OAm. Using the data in Fig. 5c and S9,† the ratio of λ is found to be 5, 9 and 6 for the Cs_2SnCl_6 NC solutions prepared from the Cs_2SnCl_6 powders prepared with the total flow rates of 0.8 mL min^{-1} (a capillary length of 20 cm), 0.4 mL min^{-1} (a capillary length of 20 cm) and 0.4 mL min^{-1} (a capillary length of 60 cm), respectively. However, the ratios of $\tilde{\tau}_1$ and $\tilde{\tau}_2$ are less than one. Such behavior is likely attributed to the difference in the radiative recombination rates of the Cs_2SnCl_6 NC solutions. It is known that both the lifetime and PLQY of the NCs are determined by using the radiative recombination rate (η_{rad}) and non-radiative recombination rate ($\eta_{non\text{-}rad}$). The average lifetime (τ_{ave}) of the NCs is calculated as[43]

$$\tau_{ave} = (A_1\tau_1{}^2 + A_2\tau_2{}^2)/(A_1\tau_1 + A_2\tau_1) = 1/(\eta_{rad} + \eta_{non\text{-}rad}) \quad (3)$$

and the PLQY is calculated as[43,44]

$$\eta = \eta_{rad}/(\eta_{rad} + \eta_{non\text{-}rad}) \quad (4)$$

which gives

$$\eta = \eta_{rad}(A_1\tau_1{}^2 + A_2\tau_2{}^2)/(A_1\tau_1 + A_2\tau_1) \quad (5)$$

with $\eta_{rad} = r_{coe}{\cdot}p{\cdot}n$ (r_{coe}, p and n are the recombination coefficient, hole concentration and electron concentration, respectively).[45] Thus, the PLQY of the NCs is determined from the radiative recombination rate and the lifetimes. With λ values in a range of 5 to 9 and $\tilde{\tau}_1$ and $\tilde{\tau}_2$ less than 1, it can be concluded that η_{rad} is larger than 1. This result reveals the important role of the volume ratio of OA to OAm in the radiative recombination rate associated with the recombination coefficient, hole concentration and electron concentration of the Cs_2SnCl_6 NCs.

The blue shift of the PL-peak wavelength of the Cs_2SnCl_6 NCs (Fig. 5a and S9†) can be attributed to the increase in the amount of OAm. Excessive OAm molecules can shear Cs_2SnCl_6 NCs into smaller ones due to the –NH– bond in OAm,[30] as illustrated in Fig. 6. Under the action of OA and OAm, smaller NCs of ~2.02 nm in average size (Fig. S12a and b, ESI†) emit blue light of shorter wavelengths due to the quantum size effect.[46,47]

The surface chemistry of the Cs_2SnCl_6 NC solutions with various volume ratios of OA to OAm is analysed on a Thermo Nicolet IS50 FT-IR spectrometer with a diamond attenuated total reflectance plate. As shown in Fig. S13 (ESI†), the peak intensity for the N–H bond centred at 1552 cm^{-1} (ref. 48) increases with the decrease of the volume ratio of OA to OAm (40 : 10 to 10 : 40), indicating an increase in the interaction between OAm and the NCs. This is in good accord with the increasing shear effect with the increase of OAm, as discussed above. The decreases in the peak intensities of the C═O bond centred at 1712 cm^{-1} (ref. 49) and the C–O bond centred at 953 cm^{-1} (ref. 50) are in line with the decrease of the volume ratio of OA to OAm from 40 : 10 to 10 : 40, which indicates the weaker interaction between OA and the NCs.

It should be noted that the PL-peak intensity and PLQY (Fig. 5c) of the Cs_2SnCl_6 NCs show a decreasing trend with decreasing NC sizes instead of the increasing trend associated with the quantum size effect.[47] This is highly due to that increasing the amount of OAm in the NC solution increases the scattering of emitted photons and blocks the light emitted from the solution. Another possible reason for the decrease of the PLQY with the increase of OAm is that decreasing the amount of OA (Fig. S11†) reduces the passivation function in controlling the surface defects of NCs,[30] which causes an ascending nonradiative recombination of holes and electrons. This is in accord with the lifetime results shown in Fig. 5d, S8 and Tables 1, S2 and S3.†

To further investigate the role of an individual ligand in controlling the PL characteristics of the Cs_2SnCl_6 NCs, the volume (50 μL) of OA was maintained constant and the volume ratio of OA to OAm was varied from 50 : 10, 50 : 20,..., to 50 : 80 in the preparation of the Cs_2SnCl_6 NC solutions in 5 mL of hexane. The as-obtained PL spectra are shown in Fig. S14a in the ESI.† The PL peak for the NC solution with a volume ratio

 This journal is © The Royal Society of Chemistry 2022

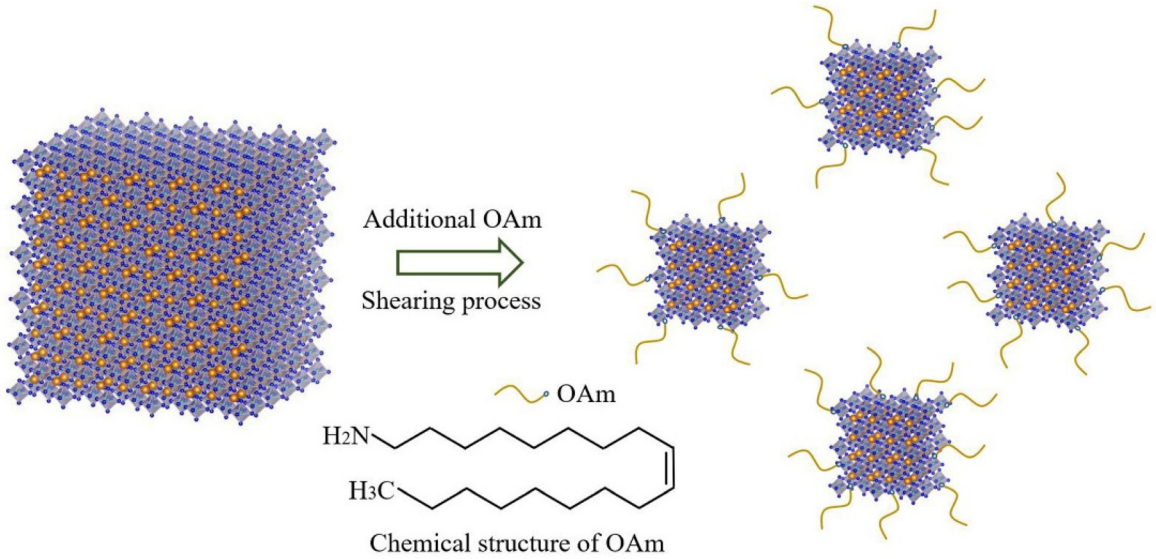

Fig. 6 Schematic for the shearing of Cs_2SnCl_6 NCs by OAm.

of 50 : 10 is centred at 437 nm; the PL peak experiences red shifts of 1 and 4 nm for the volume ratios of 50 : 20 and 50 : 30, respectively, and a blue shift with the decrease of the volume ratio from 50 : 40 to 50 : 80. The red shift of the PL peak is more likely due to the change of the interface stress/energy[51] between the ligands and the NCs caused by the increase in the OAm volume. Further increasing the OAm volume increases the contribution of the shear effect, leading to a blue shift. Fig. S14b† shows the variation of the PLQY of the Cs_2SnCl_6 NC solutions with the volume ratio of OA to OAm with 50 μL of OA, which follows a similar trend to the PL intensity, similar to the results shown in Fig. 3b and d.

The volume effects on the PL characteristics of the Cs_2SnCl_6 NC solutions were also evaluated with the volume ratios of OA to OAm of 40 : 10, 50 : 20, 60 : 30, 70 : 40 and 80 : 50 in 5 mL of hexane. As shown in Fig. S15 (ESI),† the PL-peak intensity (Fig. S15a†) and the corresponding PLQY (Fig. S15b†) decrease with the decrease of the volume ratio of OA and OAm from 50 : 20 to 80 : 50. The PL-peak wavelength fluctuates between 440 nm and 438 nm, suggesting that increasing the amount of OA in the specimen preparation can hinder the shift of the PL peak.

Considering that the Cs_2SnCl_6 NC solution prepared with a 40 : 10 volume ratio of OA to OAm exhibited the highest PLQY, we examined the long-term optical stability of the Cs_2SnCl_6 NCs in the Cs_2SnCl_6 NC solution, as shown in Fig. 7. Over a period of 60 days, the PLQY fluctuates in a range of 7.03 to 8.25 (Fig. 7a) and the PL-peak wavelength fluctuates in a range of 434 to 436 nm without a significant red or blue shift (Fig. 7b). These results support that the prepared Cs_2SnCl_6 NCs possess strong and stable optical properties.

The thermal stability (Fig. 8a–c) and UV stability (Fig. 8d–f) of the Cs_2SnCl_6 NC solution prepared with the 40 : 10 volume

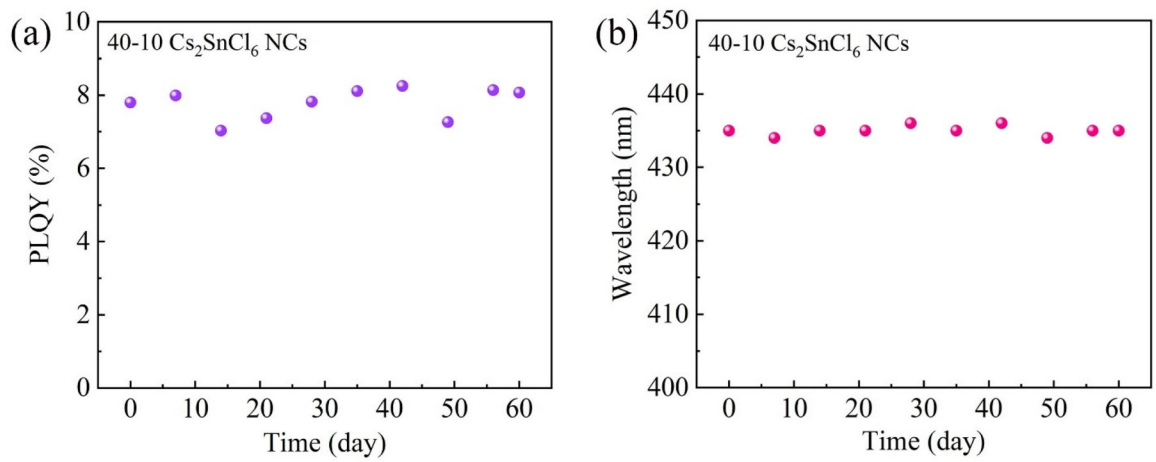

Fig. 7 Optical stability of the Cs_2SnCl_6 NC solution over a period of 60 days: (a) PLQY, and (b) PL-peak wavelength.

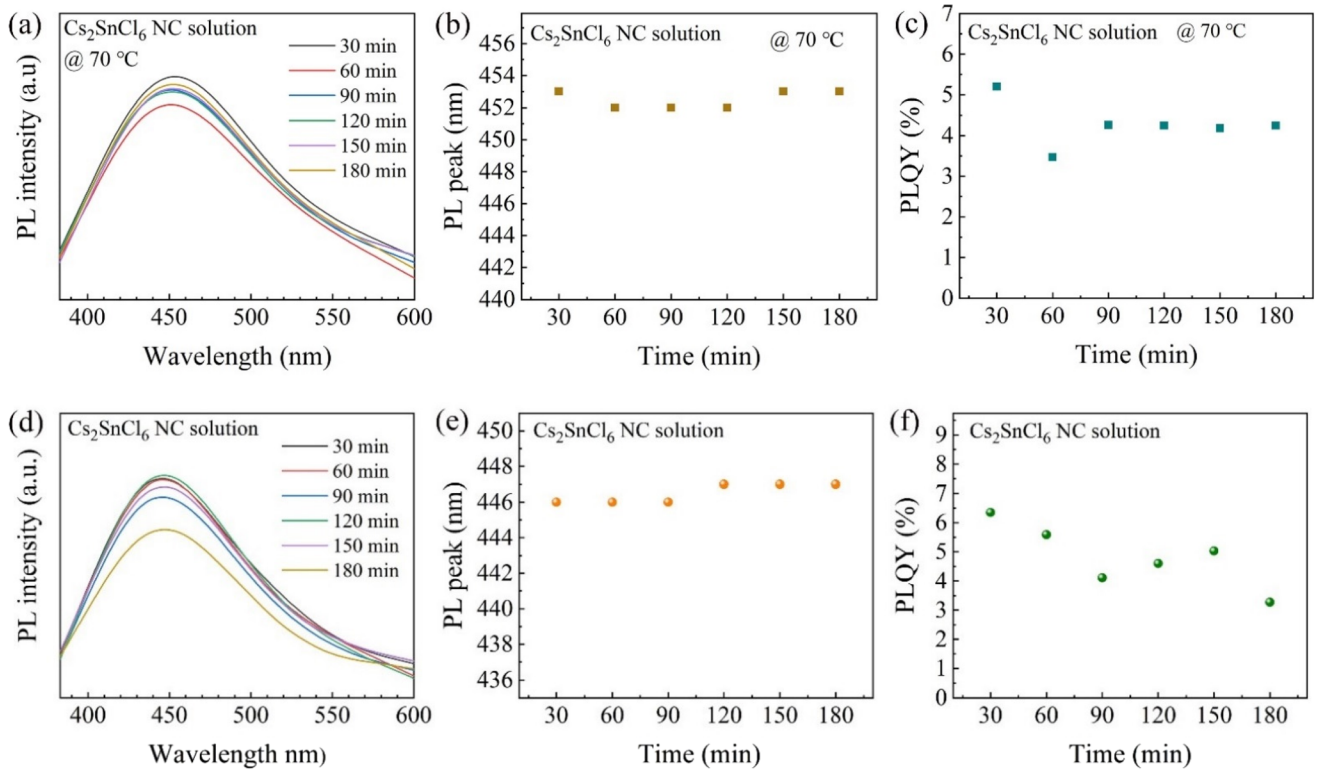

Fig. 8 (a–c) Thermal stability and UV stability (d–f) of the Cs_2SnCl_6 NC solution over a period of 180 min: (a) PL spectra of the Cs_2SnCl_6 NC solution heated at 70 °C, (b) PL-peak wavelength of the PL spectra in (a), (c) PLQY of the Cs_2SnCl_6 NC solution in (a), (d) PL spectra of the Cs_2SnCl_6 NC solution under UV light (254 nm in wavelength and 3 mW cm^{-2} irradiation rate), (e) PL-peak wavelength of the spectra in (d), and (f) PLQY of the Cs_2SnCl_6 NC solution in (d).

ratio of OA to OAm were evaluated. Fig. 8a shows the PL spectra of the Cs_2SnCl_6 NC solution heated at 70 °C over a period of 180 min. The PL peaks fluctuate in a range of 452–453 nm (Fig. 8b); the PL-peak intensity decreases with increasing heating time to 60 min, and then increases with increasing heating time from 60 to 180 min to a nearly constant value. The variation of the PLQY with the heating time (Fig. 8c) shows a nearly similar trend to the PL-peak intensity.

The PL spectra of the Cs_2SnCl_6 NC solution under UV light (254 nm in wavelength and 3 mW cm^{-2} irradiation rate) over a period of 180 min are displayed in Fig. 8d. The emission peaks centred at 446 nm for first 90 min and at 447 nm from 120 to 180 min (Fig. 8e). This result suggests that the UV stability of the Cs_2SnCl_6 NC solution is better than the thermal stability at the emission wavelength. The PLQY of the Cs_2SnCl_6 NC solution decreases from 6.35% (UV for 30 min) to 3.27% (UV for 180 min) (Fig. 8d) similar to the UV effect on the PL intensity.

We prepared three different Cs_2SnCl_6 NC solutions from the same Cs_2SnCl_6 powders with three conventionally used solvents (dichloromethane, isopropyl alcohol (IPA) and toluene (5 mL) with the 40 : 10 volume ratio of OA to OAm). Table S4 in the ESI† summaries the PL characteristics of the prepared Cs_2SnCl_6 NC solutions. The Cs_2SnCl_6 NC solutions exhibit the highest PLQY of 7.96% and the lowest PLQY of 0.46% with IPA and toluene as the solvents, respectively. The PL-peak wavelengths are 442, 446 and 450 nm for the Cs_2SnCl_6 NC solutions with IPA, dichloromethane and toluene as the solvents, respectively. Note that IPA has the highest polarity (0.546)[52] and toluene has the lowest polarity of 0.099.[52] However, it cannot be concluded that the higher the polarity, the larger the PLQY, since the PLQY of the Cs_2SnCl_6 NC solution prepared with hexane with a polarity of 0.009 as the solvent is larger than that of the Cs_2SnCl_6 NC solution with IPA as the solvent. It is the combinational effects of the solvent and ligands that determine the PL characteristics, including the PL-peak wavelength and PLQY of the Cs_2SnCl_6 NC solution.

As a green route to synthesize Cs_2SnCl_6 NCs, we used polydimethylsiloxane (PDMS) as a non-toxic ligand to synthesize Cs_2SnCl_6 NCs. Specifically, a silicone elastomer base with mass in a range of 0.01–0.05 g was used as the ligand to synthesize Cs_2SnCl_6 NCs in hexane. The PLQY of the Cs_2SnCl_6 NC solutions increases from 0.53 to 4.23% upon increasing the amount of the silicone elastomer base from 0.01 to 0.04 g. Further increasing the amount of the silicone elastomer base to 0.05 g caused the drop of the PLQY to 2.86%, as shown in Table S5 in the ESI.† This result indicates that the silicone elastomer base can be used as a green ligand in the synthesis of Cs_2SnCl_6 NCs. We also used a silicone elastomer curing agent and the mixture of the silicone elastomer curing agent and silicone elastomer base to evaluate if these materials can

 This journal is © The Royal Society of Chemistry 2022

Table 2 Comparison of blue-emitted Sn-based lead-free NCs reported in the literature and this work

Materials (LFPe NCs)	Synthesis method	Wavelength (nm)	PLQY (%)	Stability	Ref.
$CsSnCl_3$	HI	~480	0.14	14 days	12
$CsSnCl_3$	HI	475	0.17	—	62
Bi-doped Cs_2SnCl_6	Solvothermal	455	78.9	2.9% decrease of PL intensity in water in 120 min	13
Cs_2SnCl_6	HI	438	4.37	<20 s (irradiation)	63
Sb-doped Cs_2SnCl_6	HI	438/615	8.25	>20 s (irradiation)	63
Cs_2SnCl_6	HI	444	—	—	64
Cs_2SnCl_6	Microfluidics & ultrasonication	435	13.4 (Table S6, ESI†)	60 days (in air)	This work

be used as ligands to improve the PLQY of the Cs_2SnCl_6 NC solutions. However, no PLQY was detectable for the prepared NC solutions. The possible reason is that the silicone elastomer curing agent is not a capping agent that can wrap the NCs and disperse stable NCs in the solution. Also, the silicone elastomer curing agent crosslinks with the silicone elastomer base.[53,54] In this case, the silicone elastomer curing agent will prevent the silicone elastomer base from playing a role of the ligand, contributing to the formation of Cs_2SnCl_6 NCs from the Cs_2SnCl_6 powder. This might lead to that no PLQY of the NC solutions was detectable when the mixture of the silicone elastomer curing agent and silicone elastomer base was used as a possible ligand. Another possible reason for this undetected PLQY is the polarity of hexane (Table S4, ESI†), which may have a negative effect on the formation of Cs_2SnCl_6 NCs with the silicone elastomer curing agent.

Table 2 summarizes the synthesis method and the optical characteristics of blue-emitting Sn-based lead-free NCs available in the literature. It is evident that the synthesis method used in this work is very simple and the optical characteristics of the prepared Cs_2SnCl_6 NCs are superior or comparable to those reported in the literature except the Bi-doped Cs_2SnCl_6 NCs reported by Tan *et al.*[13] However, Tan *et al.*[13] used a solvothermal process, which requires a high synthesis temperature of about 200 °C and limits the amount of NCs prepared per batch.

More importantly, the Cs_2SnCl_6 NCs in hexane exhibited a remarkable stability over 60 days, which is much longer than the ones achieved by other methods. The superior stability of the Cs_2SnCl_6 NCs is likely due to the stronger Sn–Cl bond than that of some other perovskite family materials, such as $CsSnCl_3$.[55] In general, the stability of cubic Cs_2SnCl_6 will be improved when the size of the crystal decreases in a specific range. This is due to a smaller surface energy of the (100) surface, leading to a significant stability of the cubic crystal.[56] In contrast to the Cs_2SnCl_6 NCs prepared by the method presented in this work, the one prepared by hot injection experiences a thermal quenching process from a high temperature (around 150 °C) to the ice point in a mixture of ice and water. There are more structural defects in the NCs, which influence the associated optical characteristics.[57,58] That is to say, the Cs_2SnCl_6 NCs prepared by a hot injection process are at a non-equilibrium state and can experience structural relaxation at room temperature, leading to changes in the optical characteristics over a time period. Note that structural defects are also the cause of the optical instability of perovskite materials.[59–61] Fig. S16 (ESI)† shows the optical images of the fresh and 60-day' Cs_2SnCl_6 NC solutions, which show no precipitates in the Cs_2SnCl_6 NC solution after 60 days. The superior stability can likely be due to the smaller size and less defects of the Cs_2SnCl_6 NCs than the ones prepared by hot injection.

4. Conclusions

We have demonstrated the feasibility to synthesize LFHP Cs_2SnCl_6 microcrystals on a large scale on a microfluidic platform using a green aqueous solution at room temperature. Placing the LFHP Cs_2SnCl_6 microcrystals in hexane solution, we have produced blue-emitting Cs_2SnCl_6 NCs by a ultrasonication process. The experimental results reveal that the PLQY of the prepared Cs_2SnCl_6 NCs increases with increasing ultrasonication time due to the increase of the NC concentration in the solution. Decreasing the volume ratio of oleic acid to oleylamine causes the decrease of the PLQY of the Cs_2SnCl_6 NC solution and the shift of the PL-peak wavelength first to a large wavelength and then to small wavelengths. The PLQY decrease is attributed to the increase of the non-radiative recombination of charge carriers caused by the passivation loss of OA on the surfaces of the NCs. The blue shift is due to the excessive –NH– shearing effect, which reduces the sizes of large NCs. The long-term stability tests indicate that the Cs_2SnCl_6 NCs in the solution have an excellent optical stability in air over a period of 60 days without significant changes in the PLQY and PL-peak wavelength. This study provides a green-route approach for a large-scale fabrication of LFHP NCs, such as Cs_2SnX_6 (Cl, Br and I), and is expected to be extended to other lead-free NCs.

Conflicts of interest

There are no conflicts to declare.

Acknowledgements

FY is grateful for the support by the NSF through the grant CMMI-1854554, monitored by Drs Khershed Cooper and Thomas Francis Kuech, and CBET-2018411 monitored by Dr Nora F Savage.

References

1 Y. Wei, Z. Cheng and J. Lin, *Chem. Soc. Rev.*, 2019, **48**, 310–350.
2 G. W. Kim and A. Petrozza, *Adv. Energy Mater.*, 2020, **10**, 2001959.
3 H. Huang, M. I. Bodnarchuk, S. V. Kershaw, M. V. Kovalenko and A. L. Rogach, *ACS Energy Lett.*, 2017, **2**, 2071–2083.
4 C. Bi, Z. Yao, X. Sun, X. Wei, J. Wang and J. Tian, *Adv. Mater.*, 2021, **33**, 2006722.
5 M. Sulaman, S. Yang, Z. Zhang, A. Imran, A. Bukhtiar, Z. Ge, Y. Tang, Y. Jiang, L. Tang and B. Zou, *Mater. Today Phys.*, 2022, **27**, 100829.
6 Y. Chen, J. Yin, Q. Wei, C. Wang, X. Wang, H. Ren, S. F. Yu, O. M. Bakr, O. F. Mohammed and M. Li, *Nat. Photonics*, 2022, 1–6.
7 Z. Shi, J. Guo, Y. Chen, Q. Li, Y. Pan, H. Zhang, Y. Xia and W. Huang, *Adv. Mater.*, 2017, **29**, 1605005.
8 Y. Yan, T. Pullerits, K. Zheng and Z. Liang, *ACS Energy Lett.*, 2020, **5**, 2052–2086.
9 Y. Wang, J. Tu, T. Li, C. Tao, X. Deng and Z. Li, *J. Mater. Chem. A*, 2019, **7**, 7683–7690.
10 J.-M. Heo, H. Cho, S.-C. Lee, M.-H. Park, J. S. Kim, H. Kim, J. Park, Y.-H. Kim, H. J. Yun and E. Yoon, *ACS Energy Lett.*, 2022, **7**, 2807–2815.
11 F. Yuan, X. Zheng, A. Johnston, Y.-K. Wang, C. Zhou, Y. Dong, B. Chen, H. Chen, J. Z. Fan and G. Sharma, *Sci. Adv.*, 2020, **6**, eabb0253.
12 T. C. Jellicoe, J. M. Richter, H. F. Glass, M. Tabachnyk, R. Brady, S. E. Dutton, A. Rao, R. H. Friend, D. Credgington and N. C. Greenham, *J. Am. Chem. Soc.*, 2016, **138**, 2941–2944.
13 Z. Tan, J. Li, C. Zhang, Z. Li, Q. Hu, Z. Xiao, T. Kamiya, H. Hosono, G. Niu and E. Lifshitz, *Adv. Funct. Mater.*, 2018, **28**, 1801131.
14 R. Cheng, Z. B. Liang, L. Zhu, H. Li, Y. Zhang, C. F. Wang and S. Chen, *Angew. Chem.*, 2022, **134**, e202204371.
15 X. Tang and F. Yang, *Lab Chip*, 2022, **22**, 2832–2843.
16 V. Sebastian, *Nanoscale*, 2022, **14**, 4411–4447.
17 S. Marre and K. F. Jensen, *Chem. Soc. Rev.*, 2010, **39**, 1183–1202.
18 R. W. Epps, K. C. Felton, C. W. Coley and M. Abolhasani, *Lab Chip*, 2017, **17**, 4040–4047.
19 S. Kubendhiran, Z. Bao, K. Dave and R.-S. Liu, *ACS Appl. Nano Mater.*, 2019, **2**, 1773–1790.
20 I. Lignos, S. Stavrakis, G. Nedelcu, L. Protesescu, A. J. deMello and M. V. Kovalenko, *Nano Lett.*, 2016, **16**, 1869–1877.
21 Z. Bao, J.-W. Luo, Y.-S. Wang, T.-C. Hu, S.-Y. Tsai, Y.-T. Tsai, H.-C. Wang, F.-H. Chen, Y.-C. Lee and T.-L. Tsai, *Chem. Eng. J.*, 2021, **426**, 130849.
22 Y. Geng, J. Guo, H. Wang, S. D. Ling, Z. Chen, S. Chen and J. Xu, *Small*, 2022, **18**, 2200740.
23 Y. Geng, J. Guo, S. D. Ling, X. Wu, H. Liu, Z. Chen, S. Chen and J. Xu, *Sci. China Mater.*, 2022, 1–9.
24 H. Zhang, L. Zhu, J. Cheng, L. Chen, C. Liu and S. Yuan, *Materials*, 2019, **12**, 1501.
25 J. Hafizovic, M. Bjørgen, U. Olsbye, P. D. Dietzel, S. Bordiga, C. Prestipino, C. Lamberti and K. P. Lillerud, *J. Am. Chem. Soc.*, 2007, **129**, 3612–3620.
26 H. Zhang, L. Zhu, J. Cheng, L. Chen, C. Liu and S. Yuan, *Crystals*, 2019, **9**, 258.
27 A. E. Maughan, A. M. Ganose, M. M. Bordelon, E. M. Miller, D. O. Scanlon and J. R. Neilson, *J. Am. Chem. Soc.*, 2016, **138**, 8453–8464.
28 F. Yu, *Part. Sci. Technol.*, 2021, **39**, 91–100.
29 S. M. Woodside, B. D. Bowen and J. M. Piret, *AIChE J.*, 1997, **43**, 1727–1736.
30 H. Xiao, Y. Wei, P. Dang, S. Liang, Z. Cheng, G. Li and J. Lin, *J. Mater. Chem. C*, 2020, **8**, 9968–9974.
31 Y. Zhang, T. D. Siegler, C. J. Thomas, M. K. Abney, T. Shah, A. De Gorostiza, R. M. Greene and B. A. Korgel, *Chem. Mater.*, 2020, **32**, 5410–5423.
32 S. E. Creutz, E. N. Crites, M. C. De Siena and D. R. Gamelin, *Nano Lett.*, 2018, **18**, 1118–1123.
33 J. De Roo, M. Ibáñez, P. Geiregat, G. Nedelcu, W. Walravens, J. Maes, J. C. Martins, I. Van Driessche, M. V. Kovalenko and Z. Hens, *ACS Nano*, 2016, **10**, 2071–2081.
34 X. Tang, N. L. Kothalawala, Y. Zhang, D. Qian, D. Y. Kim and F. Yang, *Chem. Eng. J.*, 2021, **425**, 131456.
35 Z. Wu, M. Jiang, Z. Liu, A. Jamshaid, L. K. Ono and Y. Qi, *Adv. Energy Mater.*, 2020, **10**, 1903696.
36 D. Shi, V. Adinolfi, R. Comin, M. Yuan, E. Alarousu, A. Buin, Y. Chen, S. Hoogland, A. Rothenberger and K. Katsiev, *Science*, 2015, **347**, 519–522.
37 B. G. Yacobi and D. B. Holt, *Cathodoluminescence microscopy of inorganic solids*, Springer Science & Business Media, 2013.
38 J. T. DuBose and P. V. Kamat, *J. Phys. Chem. C*, 2020, **124**, 12990–12998.
39 Y. J. Yoon, Y. S. Shin, C. B. Park, J. G. Son, J. W. Kim, H. S. Kim, W. Lee, J. Heo, G.-H. Kim and J. Y. Kim, *Nanoscale*, 2020, **12**, 21695–21702.
40 J. Li, Z. Han, Y. Gu, D. Yu, J. Liu, D. Hu, X. Xu and H. Zeng, *Adv. Funct. Mater.*, 2021, **31**, 2008684.
41 Y. Liu, Z. Yang and S. Liu, *Adv. Sci.*, 2018, **5**, 1700471.
42 E. N. Economou, *The physics of solids: essentials and beyond*, Springer Science & Business Media, 2010.
43 B. Shu, Y. Chang, J. Zhang, X. Cheng and D. Yu, *Nano Res.*, 2021, **14**, 3352–3357.
44 I. G. Scheblykin, *Adv. Energy Mater.*, 2020, **10**, 2001724.
45 S. M. Sze, Y. Li and K. K. Ng, *Physics of semiconductor devices*, John wiley & sons, 2021.

 This journal is © The Royal Society of Chemistry 2022

46 E. Hanamura, in *Confined Electrons and Photons*, Springer, 1995, pp. 831–837.
47 L. Protesescu, S. Yakunin, M. I. Bodnarchuk, F. Krieg, R. Caputo, C. H. Hendon, R. X. Yang, A. Walsh and M. V. Kovalenko, *Nano Lett.*, 2015, **15**, 3692–3696.
48 R. Tareb, M. Bernardeau, C. Amiel and J.-P. Vernoux, *FEMS Microbiol. Lett.*, 2017, **364**, fnw298.
49 K. Fahmy, F. Jäger, M. Beck, T. A. Zvyaga, T. P. Sakmar and F. Siebert, *Proc. Natl. Acad. Sci. U. S. A.*, 1993, **90**, 10206–10210.
50 J. Huberty and R. Madix, *Surf. Sci.*, 1996, **360**, 144–156.
51 F. Yang, *Phys. Lett. A*, 2022, **428**, 127931.
52 C. Reichardt and T. Welton, *Solvents and solvent effects in organic chemistry*, John Wiley & Sons, 2010.
53 J. Schweitzer, S. Merad, G. Schrodj, F. Bally-Le Gall and L. Vonna, *J. Chem. Educ.*, 2019, **96**, 1472–1478.
54 Z. Wang, A. A. Volinsky and N. D. Gallant, *J. Appl. Polym. Sci.*, 2014, **131**.
55 Z. Xiao, H. Lei, X. Zhang, Y. Zhou, H. Hosono and T. Kamiya, *Bull. Chem. Soc. Jpn.*, 2015, **88**, 1250–1255.
56 A. S. Barnard and P. Zapol, *J. Chem. Phys.*, 2004, **121**, 4276–4283.
57 M. A. Reshchikov, *Phys. Status Solidi A*, 2021, **218**, 2000101.
58 I. Buyanova, W. Chen, G. Pozina, B. Monemar, W.-X. Ni and G. Hansson, *Appl. Phys. Lett.*, 1997, **71**, 3676–3678.
59 S. Chen, X. Wen, S. Huang, F. Huang, Y. B. Cheng, M. Green and A. Ho-Baillie, *Sol. RRL*, 2017, **1**, 1600001.
60 A. Hassan, Z. Wang, Y. H. Ahn, M. Azam, A. A. Khan, U. Farooq, M. Zubair and Y. Cao, *Nano Energy*, 2022, 107579.
61 B. W. Park and S. I. Seok, *Adv. Mater.*, 2019, **31**, 1805337.
62 C. Kang, H. Rao, Y. Fang, J. Zeng, Z. Pan and X. Zhong, *Angew. Chem.*, 2021, **133**, 670–675.
63 Y. Jing, Y. Liu, J. Zhao and Z. Xia, *J. Phys. Chem. Lett.*, 2019, **10**, 7439–7444.
64 A. Veronese, M. Patrini, D. Bajoni, C. Ciarrocchi, P. Quadrelli and L. Malavasi, *Front. Chem.*, 2020, **8**, 35.

This journal is © The Royal Society of Chemistry 2022